HHS Public Access

Author manuscript

Small. Author manuscript; available in PMC 2018 October 01.

Published in final edited form as:

Small. 2017 October ; 13(37): . doi:10.1002/smll.201701300.

Photoacoustic-Guided Surgery with Indocyanine Green-Coated Superparamagnetic Iron Oxide Nanoparticle Clusters

Jayesh P. Thawani, MD[1,2,†], **Ahmad Amirshaghaghi, PhD**[2,†], **Lesan Yan, PhD**[2], **Joel M. Stein, MD, PhD**[2,3], **Jessica Liu**[2], and **Andrew Tsourkas, PhD**[2,*]

[1]Department of Neurosurgery, Hospital of the University of Pennsylvania, Philadelphia, Pennsylvania 19104

[2]Department of Bioengineering, School of Engineering and Applied Sciences, University of Pennsylvania, Philadelphia, Pennsylvania 19104

[3]Department of Radiology, Division of Neuroradiology, Hospital of the University of Pennsylvania, Philadelphia, Pennsylvania 19104

Abstract

A common cause of local tumor recurrence in brain tumor surgery results from incomplete surgical resection. Adjunctive technologies meant to facilitate gross total resection have had limited efficacy to date. Contrast agents used to delineate tumors pre-operatively cannot be easily or accurately used in the real-time operative setting. Although multimodal imaging contrast agents have been developed to help the surgeon discern tumor from normal tissue in the operating room, these contrast agents are not readily translatable. We have developed a novel contrast agent comprised solely of two FDA-approved components, indocyanine green (ICG) and superparamagnetic iron oxide (SPIO) nanoparticles - with no additional amphiphiles or carrier-materials, to enable pre-operative detection by MRI and intraoperative photoacoustic (PA) imaging. The encapsulation efficiency of both ICG and SPIO within the formulated clusters is ~100% and the total ICG payload is 20–30% of the total weight (ICG + SPIO). The ICG-SPIO clusters are stable in physiologic conditions, can be taken up within tumors by enhanced permeability and retention, and are detectable by MRI. In a pre-clinical surgical resection model in mice following injection of ICG-SPIO clusters, animals undergoing PA-guided surgery demonstrated increased progression-free survival compared to animals undergoing microscopic surgery.

Summary

A novel contrast agent was developed that is comprised solely of two FDA-approved components, indocyanine green and superparamagnetic iron oxide nanoparticles - with no additional amphiphiles or carrier-materials, to enable pre-operative detection of tumors by MRI and intraoperative photoacoustic imaging. Tumor-bearing mice that underwent PA-guided surgery demonstrated increased progression-free survival.

[*]Corresponding Author: Andrew Tsourkas, PhD, atsourk@seas.upenn.edu, Phone: 215-898-8167, Fax: 215-573-2071, Address: 210 S. 33rd Street, 240 Skirkanich Hall, University of Pennsylvania, Philadelphia, PA 19104.

[†]These authors contributed equally to this work.

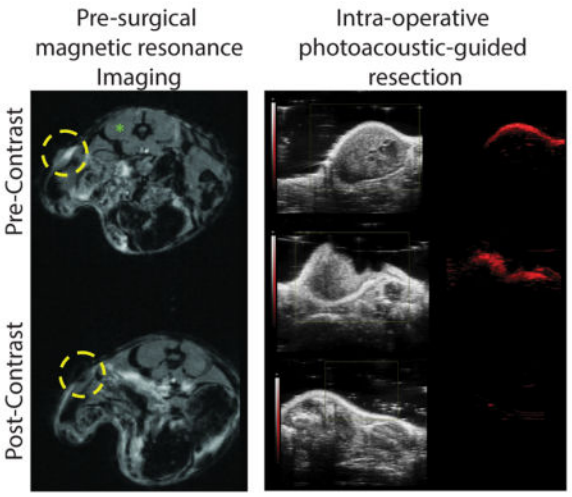

Keywords

indocyanine green; superparamagnetic iron oxide; magnetic resonance imaging; photoacoustic imaging; image-guided surgery

Introduction

Incomplete tumor resection is a common cause of local tumor recurrence following surgery of intrinsic brain tumors. In some areas of the body, margins may be taken and studied microscopically in real-time in order to better ascertain whether adequate margins around a tumor's boundaries have been obtained. With microscopically invasive tumors and those in surgically unforgiving areas of the body like the central nervous system, it is important for the surgeon to understand which areas represent functional or normal regions within the context of an infiltrating, oncological process. Glioblastoma multiforme, the most common (and lethal) primary brain tumor, exhibits a rapid and destructive growth pattern in the brain[1]. Patient outcomes strongly correlate with the extent of surgical resection based on multiple published series in the literature[2–7]. At the time of an operation, surgeons typically use visual inspection and tactile feedback to discriminate tumor margins from surrounding normal brain tissue. For pre-operative planning, magnetic resonance (MR) imaging is used in order to ascertain a tumor's margins (given that these tumors enhance with the administration of gadolinium). Even with adjunctive technologies such as intraoperative MRI, MR-based navigation techniques, and ultrasound, there remains a high rate of local failure[1].

Fluorescence imaging techniques have been developed in the last several decades to aid in cancer imaging. At present, however, only three fluorescent contrast agents (methylene blue, fluorescein sodium, and indocyanine green (ICG)) are approved for use in humans by the United States Food and Drug Administration (FDA)[8]. Of these compounds, ICG is unique in that its excitation/emission spectra lie in the near-infrared (NIR) range. This allows for selective imaging, as fewer effects from the autofluorescence of native tissues and blood interfere with NIR imaging (as compared to conventional fluorescence imaging in the visible

spectrum), even through deep tissues[9]. As an amphiphilic cyanine dye with low toxicity, ICG can be safely injected intravenously[10]. Following injection, it is rapidly adsorbed onto plasma proteins and is cleared in the liver. Unfortunately, ICG alone as a contrast agent has several shortcomings: it has a short half-life in circulation on the order of minutes, its fluorescence decreases due to photobleaching and degradation, and it does not possess functional groups or cell specificity[11,12]. Nevertheless, numerous pre-clinical and clinical studies utilizing ICG as a NIR fluorescent contrast agent have been published[9]. ICG is presently used in clinical vascular imaging applications examining blood flow in real-time. With optimization of dosing and fluorescence imaging techniques, ICG was employed by thoracic surgeons to delineate lung tumors[13–15]. Although ICG has recently been demonstrated as a cancer imaging adjunct through NIR fluorescence imaging in human brain tumors, the positive predictive values associating fluorescence with the presence of tumor on pathological specimens are suboptimal[16].

Photoacoustic (PA) imaging utilizes pulsed laser excitation to promote thermoelastic expansion of tissues or contrast agents in the MHz range. Excitation occurs through deep, opaque tissues in the visible and NIR spectra with real-time imaging mediated via an ultrasound platform/transducer[17]. Using ICG as a PA imaging contrast agent allows for deep tissue imaging in real-time[18–20]. It further allows us to differentiate its presence from blood, as oxy and deoxy-hemoglobin can interfere with detection even in the NIR fluorescence range. By combining ICG with superparamagnetic iron oxide (SPIO), a low-cost FDA-approved agent, we developed a stable nanoparticle cluster that is taken up *in vivo* by enhanced permeability and retention (EPR); as such, it is both detectable by MR and PA imaging modalities. Importantly, the PA imaging agent is stably associated with the MRI-detectable SPIO, thus allowing the preoperative contrast-enhanced radiologic findings to be directly related with the visual presentation of PA-enhanced pathology during surgery. The surgeon is able to delineate areas of contrast enhancement based on preoperative MR imaging in real-time using PA imaging, despite the presence of blood and without concern for background signal (autofluorescence) or rapid clearance from the circulation. The goals of the present study were to establish a model to demonstrate the proof-of-principle showing that a single contrast agent as described could be detected by both PA and MR imaging; secondly, we established an invasive tumor model and tested the hypothesis that surgery mediated by PA imaging could lead to improved rates of progression-free survival in mice bearing tumors that recapitulate the growth of glioblastoma.

Results

Preparation and characterization of indocyanine green-coated superparamagnetic iron oxide clusters

Indocyanine green (ICG)-coated superparamagnetic iron oxide (SPIO)-nanoparticle clusters (ISCs) (Fig. 1) were formed via an inverse emulsion with ICG and SPIO nanoparticles (diameter = 7.3±1.0 nm; Fig. S1) in the oil-phase. No additional amphiphiles (e.g. polymers, surfactants, etc) or other carrier-materials were included in the emulsion. The generated ISCs are soluble in water, with ICG acting as the amphiphilic solubilizing agent (Fig. 1A). The synthetic approach is highly reproducible (Table S1), resulting in ISCs that have an

average diameter of 96.87±7.8 nm and a polydispersity (PDI) index of <0.18 (based on dynamic light scattering, DLS) (Fig. 1B). ISCs are visible on TEM as densely packed clusters of SPIO nanoparticles (Fig. 1B, inset). The loading efficiency is >95% for SPIO and >90% for ICG, when the ICG:Fe ratio (w/w) is in the range of 1:4 to 1:3 (Table S2). A further increase in the ratio of ICG:Fe during micelle formation does not result in significantly more ICG per cluster, but rather just a reduction in the ICG encapsulation efficiency. Accordingly, regardless of the starting ICG:Fe ratio (w/w), from 1:4 to 2:1, the resultant ISCs have remarkably similar physical-chemical properties. The final payload of ICG for each of the synthetic conditions tested was 20–30% of the total weight (ICG + Fe).

The ISCs are highly stable in water, with no observable change in size over 8 days, based on DLS measurements (Fig. 1C and Fig. S2). Relaxometry measurements revealed an average r2 value of 318±3 $mM^{-1}s^{-1}$ and MR images of a phantom confirmed strong T2 contrast relative to controls (Fig. 1D). Given the high concentrations of ICG and SPIO present in the final nano-formulation, ISC fluorescence is extremely low, due to both self-quenching and iron-mediated quenching (Fig. S3); however, a robust photoacoustic (PA) signal is detectable, even when ISCs within polyethylene tubing are submerged at a depth of 1–2 cm in an aqueous (e.g. water) fluid (Fig. 1E). Spectral analysis of ISC absorbance and the PA signal reveals a red-shifted peak (~835 nm), relative to the absorbance peak of free ICG (~780 nm; Fig. S4).

Evaluation of ISCs within biological samples

To evaluate the stability of ISCs under physiological conditions, the ISCs were diluted in fetal bovine serum (FBS) and kept at 37°C under constant shaking. A slight (~10nm) increase in the hydrodynamic diameter of ISCs was observed immediately after addition to serum, consistent with some protein absorption. However, no aggregation or precipitate was observed and there was no significant change in the T2 relaxation time (Fig. 2A). Approximately 20% of the surface-bound ICG was released from the ISCs within the first few hours after addition of serum, but then no further release was detectable for up to 48 hours (Fig. 2B). These findings suggest that the ICG forms a highly stable interaction with the SPIO surface.

The cytotoxicity of the ISCs was examined in an MTT cell proliferation assay. Specifically, increasing concentrations of ISCs were incubated with U251 glioblastoma cells, human umbilical vein endothelial cells (HUVEC), and human embryonic kidney (HEK) 293T cells. It was found that the ISCs had no effect on the proliferation of any of the cells tested, up to a concentration of 0.24 mg Fe/mL (Fig. 2C).

To evaluate the potential cytotoxicity of ISCs in mice, histological analysis was performed on the liver, spleen and kidney 1 day following the injection of ISCs (1 mg/kg, based on ICG weight) into C57BL/6J mice. Hematoxylin and eosin (H&E) staining of these organs showed no evidence of abnormal pathology or adverse effects (Fig. S5)

Small animal imaging: magnetic resonance and photoacoustic imaging

To assess the contrast-enhancing capabilities of ISCs in a murine tumor model, the human glioblastoma cell line U251 was selected and implanted in the flank of athymic nude mice.

U251 tumors exhibit gross pathologic evidence of tumor myoinvasion (noted with tumor growth > 7 mm in size) (Fig. S6). Nests of tumor cells were evident throughout the adjacent musculature. The U251 cells were engineered to express firefly luciferase, to allow tumor cells to be detected in live animals (for recurrence studies).

MR imaging before and 24 hours after injection of 1 mg/kg ISCs (based on ICG weight) revealed a notable loss in signal (i.e. hypointensity) in the flank tumors following injection (Fig. 3A and Fig. S7), consistent with the accumulation of SPIO nanoparticles. Tumor-specific accumulation of ISCs is likely a consequence of enhanced permeability and retention (EPR) and has been demonstrated at 24 hours following intravenous injection[16,21–23]. Signal-to-background (SBR) measurements were made using the tumor and the paraspinous musculature as background. The post-injection SBR was significantly lower at 0.12 +/− 0.03 compared to pre-injection SBR of 1.03 +/− 0.14, $p<0.001$ (Fig. 3B).

ISCs were also detectable via PA imaging, 24 hours post-injection (1 mg/kg), as noted by the appearance of a signal with a peak wavelength at ~850 nm (ultrasound gain +27 dB, PA gain, 25 dB, priority 95%) (Fig. 3C). No PA signal was observed pre-contrast. The PA signal was often limited to the outer surface of the tumor and was not always detectable throughout the entire tumor mass; however, partial resection of the tumor showed that the ICS nanoclusters were in fact present within the tumor core (Fig. 4A). This suggested that ICSs could be used to detect residual tumor tissue during surgery and further supported the use of ISCs for image-guided surgery.

Notably, the ISCs within the tumor were also detectable via fluorescence (Fig. S8), 24 hours post-injection, despite the significant degree of quenching in the stock formulation. The fluorescent signal within the tumor was significantly more robust than in animals injected with an equivalent dose of free ICG, likely because of higher ISC accumulation at this time point.

Evaluating recurrence following surgery: comparing resection mediated by PA imaging to microscopic surgical resection

A randomized, blinded surgical trial to evaluate recurrence following two surgical methods was performed. Thirty athymic nude female mice were implanted with U251(Luc+) cells in the right dorsal flank. Of these, 24 demonstrating suitable tumor growth were selected and randomized 4 weeks after implantation into two groups (PA-guided surgery arm, N=12; microscopic surgery arm, N=12) in order to closely match tumor sizes between groups. The mean animal weights were 26.2 g (24–30 g) in the PA cohort and 27.5 g (23.1–31.2 g) in the microsurgery cohort. The mean largest dimension in terms of tumor size was 1.1 cm (0.7–1.3 cm) in the PA cohort and 1.0 cm (0.6–1.1 cm) in the microsurgery cohort.

Photoacoustic imaging performed prior to injection (850 nm) showed minimal/no PA signal within tumors. Twenty-four hours after intraorbital injection of ISCs (1 mg/kg based on ICG weight), PA imaging was performed; tumors demonstrated uptake based on PA imaging with excitation set at 850 nm. All animals were injected with ISCs at the same dose. No immediate toxicity was observed during the surgical procedure or in the perioperative period. Surgical resection was performed in both groups by a neurosurgeon under 3.5X

magnification with bright white lighting. A combination of forceps and sharp dissection was carried out in order to completely resect the tumors. Where tumors involved the flank musculature, efforts were made to resect the tumor completely from the muscle. After gross tumor resection, the mice in the microscopic surgical resection cohort had their wounds irrigated with 0.9% normal saline. The mice in the PA-guided surgery cohort similarly underwent surgical resection aimed at gross total resection. Following irrigation, however, PA imaging was performed. In 10/12 animals, additional tumor tissue was identified and additional surgery was carried out to completely remove tumor. Resection proceeded until PA average was <50% of pre-operative value at 850 nm and post-resection spectra matched that of background tissue in the flank. For all animals, imaging parameters and time-gain constant were maintained at the same level. Following skin closure, 8/12 animals in the PA-guided surgery cohort and 7/12 animals in the microscopic surgery cohort had seromas noted at the site of surgery. No drains were placed. These seromas were all fluctuant and not solid or nodular in appearance.

Animals were tagged and identified following the surgical procedure by another individual; injection of D-Luciferin and bioluminescence studies were also carried out blinded to the surgeon. Animals were imaged through bioluminescence imaging at four time points (Fig S9 and S10). Recurrence was noted based on the appearance of bioluminescence 12 minutes following injection of D-luciferin for each animal. In the PA-guided surgery cohort, 3/12 animals demonstrated recurrence noted at t=25 days and no additional recurrent tumors were detected through 42 days. All three animals that developed recurrence were from the group that had tissue removed following PA-guided surgery. The two animals that did not have additional tumor identified at the time of PA imaging (following first-stage surgical resection) did not develop recurrent tumor. All animals survived.

In the microscopic surgical resection cohort, 4/12 animals showed recurrent tumors at 25 days and 8/12 animals showed recurrent tumors by 42 days. 2/12 animals died (t=10 and t=25). The PA-guided surgical resection cohort (N=12) demonstrated improved progression-free survival at an endpoint of 42 days as compared to the microscopic surgical resection cohort (N=12) based on the log-rank test (p=0.0053) (Fig. 4B).

Discussion

We present a simple method to utilize ICG and SPIO—two low-cost, FDA-approved components—in order to generate stable clusters in solution. The amphiphilic properties of ICG allow for the orientation of ringed, non-polar groups medially toward the hydrophobic SPIO cores, leaving the hydrophilic/polar ends of the molecule oriented toward the outer part of the construct. Our data suggest that the association between ICG and SPIO in this nanoparticle cluster is robust—even in physiologic conditions. Although several authors have described constructs using di-block polymers or reverse emulsion techniques to contain ICG and SPIO[24–26], the translatability of these engineered nanoparticles remains a question. Based on our work, uptake mediated by EPR into U251 flank xenografts demonstrates the presence of both ICG and SPIO through the use of Photoacoustic imaging and MR imaging, respectively. ISCs can be delineated from normal tissues, including oxy- and deoxy-hemoglobin given the red-shifted peak wavelength of excitation (~850 nm)

relative to that observed with fluorescence, decreasing auto-excitation of normal tissues. Quenching with increasing concentrations of excitable compounds, as is observed with fluorescence excitation, is not observed with PA imaging. Given the safety and regulatory status of both ICG and SPIO, ISCs have the benefit of translatability and potential for use in patients.

The present study using ISCs demonstrates a simple concept—that a T2-based MR contrast agent can be visualized *in vivo*, in real-time by PA imaging. Short of cell-specific contrast agents, which are disappointingly scarce in the treatment of humans, this represents a first step for clinicians in directly utilizing MR imaging for surgical planning and treatment. Intraoperative adjunctive technologies, such as imaging-based navigational systems have been useful in allowing the surgeon to estimate areas of contrast enhancement, which likely represent tumor (owing to breakdown of the blood-brain barrier). These technologies rely on a static pre-operative image. Unfortunately, changes in the surgical cavity (loss of cerebrospinal fluid, deformation/creation of a surgical cavity or “brain shift”, and diuresis) render pre-operative imaging less accurate. Intraoperative MR imaging techniques allow the surgeon to perform surgery in or near an MRI scanner, with usually a single imaging update[27,28]. In terms of problems with intraoperative MRI, the timing and dose of contrast administration remain individualized and not optimized. Surgeons are essentially violating the blood brain barrier that contrast agents pass through. As a result, otherwise non-enhancing areas may enhance due to surgical intervention. Increased surgical time and costs associated with MR imaging platforms also remains a problem. Lastly, some studies looking at survival and progression-free survival have not shown a clear benefit with intraoperative MRI[29,30].

For the last two decades, intraoperative fluorescent contrast agents have been proposed to aid the neurosurgeon in identifying tumor tissue during surgery. The most popular approach has been fluorescent-guided intraoperative imaging with 5-aminolevulinic acid (5-ALA). 5-ALA is a pro-drug in the porphyrin family that facilitates tumor identification; its use improves gross total resection rates and prolongs progression-free survival in patients with high-grade gliomas[3]. Despite its benefits, 5-ALA has not reached widespread popularity in the United States, because it has limitations including low depth of penetration, autofluorescence from surrounding tissues, and issues with elevated liver enzymes following administration[31,32]. Despite FDA approval for other indications, 5-ALA is not yet approved as an imaging adjunct in treating patients with brain tumors. Current FDA-approved fluorescent contrast agents include methylene blue, fluorescein sodium, and indocyanine green (ICG)[8]. In general surgery, methylene blue is used to identify parathyroid glands during parathyroidectomies. Unfortunately, methylene blue loses color and fluorescence rather rapidly in physiologic conditions, and high doses have been associated with cardiotoxicity[33]. Fluorescein is approved for use with retinal angiography and can be used off-label to monitor fluid filled structures as a contrast agent. Although fluorescein is used in neurosurgery, its dosing has not been optimized and its emission wavelength is in the range where autofluorescence—or fluorescence of native tissues— interferes with visualization[34]. Both fluorescein and methylene blue fluoresce in the visible spectrum (emission wavelengths of 520 nm and 680 nm, respectively). ICG allows for a greater depth

of detection and is less susceptible to autofluorescence of surrounding tissues given that it absorbs/emits in the near-infrared range[23].

The FDA has approved ICG for use since its development by the Kodak Corporation in the 1950s. Its use in cancer imaging, however, has been hindered by unfavorable pharmacokinetics and detection by fluorescence. As a near-infrared contrast agent, ICG has a high sensitivity and a low autofluorescence background. Although ICG has a favorable depth of detection in the brain given these attributes, it has a short half-life in circulation (2–4 minutes), binds rapidly to plasma proteins, undergoes fluorescence photobleaching, is thermally unstable, and lacks functional or cell-specific targeting groups. Using ICG as an absorbing agent with high concentrations of SPIO (necessary for paramagnetism and detection by MR imaging) renders it a less useful as a fluorescent contrast agent due to quenching of the fluorescent yield. Detection by PA imaging allows for the detection of ICG at high concentrations. The photoacoustic effect in theory dictates that signal should increase with concentration; this matches our observation with a linearly increasing average signal with concentration. As blood and surrounding tissues can interfere with NIR fluorescence detection with ICG, PA imaging demonstrates an even further red-shift in peak excitation making ISCs a favorable contrast agent in the body.

After demonstrating that this contrast agent could be used *in vivo* in mice, we sought to develop a surgical model that recapitulates the invasive properties of certain tumors like glioblastoma. The U251 cell line was chosen based on several studies[35–38] and our experience in working with this tumor cell line. We found that when tumors grew to a certain size (> 7 mm in largest dimension), invasion into the flank occurred, which was confirmed by histopathology. Creating a randomized, blinded trial allowed us to assess the recurrence patterns following surgery in two cohorts – one undergoing surgery conventionally (using bright light and microscopy) and the other undergoing surgery with the use of PA imaging. Both cohorts received ISCs in the same dosing scheme. Toxicity did not appear to be an issue in either cohort. In reports, those with iodine allergies may demonstrate a reaction to ICG[16].

There are several shortcomings to make clear. First, ISCs are not cell-specific. We utilized uptake via EPR in demonstrating the proof-of-concept that two FDA-approved compounds could comprise a contrast agent detectable by both MR and PA imaging modalities. Our next steps include utilizing ISCs and packaging them with cell-specific constructs and moieties. Our study utilized a 9.4-Tesla MRI, which is not currently utilized in humans outside of research, but susceptibility-weighted sequences are highly sensitive to iron oxide at clinical field strengths and SPIO nanoparticles have been used successfully in multiple clinical trials. Although photoacoustic imaging platforms are just starting to be used in humans in the clinical setting, they are not yet widely utilized. Our contrast agent demonstrated hypointensity on MR imaging; the T1 sequence with gadolinium administration is the main sequence used at present to delineate brain tumors in humans. The surgical model of glioblastoma described in the present study used may not recapitulate the incredible degree of invasiveness and necrosis noted in the brains of some patients. Although we have been able to produce intracranial models in mice, surgery performed to remove tumors in a small

animal can be a morbid procedure. In the future, we plan on developing larger animal models for surgical resection, recurrence, and survival studies.

In conclusion, we developed a novel contrast agent comprised entirely of FDA-approved components that is detectable by MR and PA imaging in real-time. ICG SPIO clusters are stable in *in vitro* and in physiologic conditions, can be taken up within tumors by EPR, and are detectable in a preclinical animal model 24 hours following injection. In a surgical resection model following injection of ISCs, animals undergoing PA-guided surgery demonstrated increased progression-free survival compared to animals undergoing microscopic surgery. Further efforts will incorporate ISCs into cell-specific technologies and will contribute to wider usage of photoacoustic imaging in surgery.

Experimental Section

Superparamagnetic Iron Oxide (SPIO) Synthesis

SPIO nanoparticles were prepared by thermal decomposition as previously described[39–41] with some modifications as noted here. Briefly, iron(III) acetylacetonate [Fe(acac)3] (2mmol), 1,2-hexadecanediol (5mmol), oleic acid (2mmol), and oleylamine (6mmol) and benzyl ether (20 mL) were stirred under nitrogen. The mixture was heated to 200 °C for 15min, and then under a blanket of nitrogen, heated to reflux (300 °C) for 1h. After allowing the reaction to cool to room temperature, two volumes of ethanol were added and the resulting mixture was centrifuged (5500g × 15min) to precipitate the nanoparticles. The particles were then allowed to air dry and dissolved in toluene. Large aggregates were removed by centrifugation at 3000g × 15min.

ICG SPIO Cluster Synthesis

A mixture (200 μL) containing indocyanine green (ICG) (2mg into dimethylformamide) and SPIO (1.1, 2.2, 4.4, 6.6, and 8.8 mg based on the Fe concentration in toluene) was pipetted into a glass vial containing 4 mL of water, and the sample was sonicated until a homogenous solution was observed. The toluene was evaporated overnight. Dialysis was performed in 4L of water to remove dimethylformamide. The ISCs were purified by passing through a MACS® (25 LD columns, Miltenyi Biotec, Germany) column. Finally, the purified clusters were characterized by UV-absorption spectroscopy (Varian, 100 Bio), plasma optical emission spectroscopy (ICP-OES) (Spectro Genesis, GMBH) DLS (Malvern, Zetasizer, Nano-ZS), TEM (JOEL 1010) analysis, and relaxometry (Bruker, mq60 NMR analyzer). The ICG and SPIO encapsulation efficiency (EE) was calculated according to the following equation:

$$\text{Encapsulation efficiency}\,(\%) = \frac{\text{Weight of ICG in purified nanoparticles}}{\text{Weight of ICG used in synthesis}} \times 100$$

ICG and Iron concentration were quantified by UV-absorption and ICP-OES, respectively.

ISC Release and Stability Studies

The amount of ICG adsorbed on ISCs in fetal bovine serum (FBS) was determined based on absorbance measurements. A 1:10 dilution of ISCs in water:FBS solution was prepared and stored in the dark at 37°C with shaking. The pH was 7.4 for mixtures. Aliquots were run through MACS columns to separate ICG released (ICG bound to serum proteins + free) from that still adsorbed onto SPIO cores. 'Free ICG' as it is stated in the manuscript considers ICG that is not associated with the SPIO cores and exists bound to serum proteins (majority) or in free form. The peak absorbance spectra of ICG in the particle-adsorbed compartment was determined by dissolving ISCs in DMF (dissolving free ICG in DMF). Normalized peak absorbance was measured over time. Release of ICG from ISCs was measured, over time, as a fraction of the total amount of ICG in ISCs at t=0. Absorbance was used to determine the amount of ICG in solution (based on a standard curve of ICG in DMF). In addition, DLS was used to measure the particle size based on mean intensity (%) measurements taken over a total of 8 days in water and FBS. Finally, ISCs were incubated in water and FBS at 37°C. Aliquots taken from the sample (ISCs:solvent) were tested for magnetic properties (T2 mode).

MTT assay

U251 human glioblastoma cells (2.6×10^4 cells per well) were seeded in 96-well plates and incubated overnight to allow the cells to attach to the surface of the wells. The cells were then mixed with increasing concentrations of ISCs for 24 hrs and the cell viabilities were determined by a standard MTT assay[42].

Cell Line Selection and Initial Animal Studies

Athymic nude female mice (aged 6 weeks) were utilized for the study (n = 12). U251 human glioma cells expressing firefly luciferase (U251 +Luc) were utilized for (1) the invasive phenotype observed across studies [36–38,43] and (2) ease of detection by bioluminescence[44]. U251 demonstrates the histological and MR imaging characteristics of glioblastoma as seen clinically in humans[45]. These cells were cultured and implanted in the right flank as previously described protocols [44,46,47]. Briefly, cells were passaged in DMEM with antibiotics (1% penicillin/streptomycin). Non-enzymatic dissociation media was used. 5×10^6 cells were implanted in the right flank of the mice at approximately 6–8 weeks of age; animals were observed every 4 days to evaluate tumor growth. In a subset of animals, bioluminescence testing was undertaken to confirm peak timing in terms of administration of D-luciferase[44]. Dose testing (0.25, 1, 5 mg/kg ICG in ISCs injected intraorbital) was performed with no toxicity observed in animals. Visualization by *in vivo* fluorescence imaging and MR imaging (9T) confirmed the presence of ISCs at 24 hours. Equivalent concentrations of ICG free dye were also evaluated. Instrumentation/parameters: Perkin Elmer IVIS Spectrum In Vivo Imaging System (excitation 745 nm, emission 800 nm, lamp level = low, exposure times: (A) 1, (B) 3, (C) 10, binning 4, f=1). Bioluminescence studies were performed 12 minutes following IP injection of D-luciferin sodium salt based on peak signal time (200 uL, 15 mg/ml intraperitoneal injection)[47].

All animals in the present study were anesthetized according to an approved IACUC protocol (1–2.5% inhalational isofluorane with meloxicam dosed 5–10 mg/kg subcutaneous

given every 12–24 hours) and euthanized by CO_2 inhalation/cervical dislocation. Animals were monitored by regular staff and by veterinarians if they demonstrated illness outside of protocol. Histology was performed using hematoxylin and eosin staining. Tumors were surgically removed and resection sites were catalogued for gross pathologic findings. In a group of 12 mice with U251 orthotopic flank xenografts, only 1 of 4 animals (25%) with tumors less than 7 mm in size exhibited myoinvasion on histology as compared to 100% of 8 animals with tumors > 7 mm in size showing histologic evidence of myoinvasion.

Fluorescence Imaging

Serial 1/2x dilutions from [5 μg/ml] to 1/16x [0.31μg/ml] of ISCs were used in a 120-well plate as a phantom. An equivalent amount of ICG was used as control. Images were acquired with a Perkin Elmer IVIS Spectrum In Vivo System (excitation 745 nm, emission 800 nm, lamp level = low, exposure time = 10s, binning 4, f=1).

MRI Phantom and Animal Imaging by MRI

Relaxometry measurements were performed in T2* mode (Varian, 9.4 Tesla); Iron concentration was quantified by ICP-OES. A plastic 120-well plate (MR phantom) was used in order to test the T2 hypointensity associated with ISCs compared to control (free ICG at equivalent concentrations) on a 9T magnet. [Fe] concentrations were as follows: 1, 0.5, 0.25, 0.125, and 0.0625 mM. Mice bearing U251 flank xenografts were injected with 1 mg/kg ISCs via intraorbital injection. Imaging was performed 24 hours after injection. Contrast enhancement on T2*-weighted imaging (seen as hypoenhancement following injection of ISCs) was quantified using ImageJ. Pre- and post-injection imaging parameters (gems, TR200, TE3, 1 avr) were matched and confirmed by an attending radiologist. Imaging analyses were performed on T2-weighted imaging sequences, using the tumor (signal) and the paraspinous musculature as background. Comparison of means testing was performed to compare the mean SBRs of animals pre-injection versus post-injection.

Photoacoustic Phantom and Animal Imaging

Photoacoustic (PA) testing on the Vevo Lazr device (VisualSonics, Toronto CA) was performed in 0.5 mm diameter polyethylene tubing submerged in water at a depth between 1–2 cm. Samples were injected (50 uL) into the tubing prior to imaging. Spectra and imaging data were collected. ISCs were tested according to ICG concentrations (0.5, 0.45, 0.40, 0.35, and 0.3 mg/mL) with the following settings: ultrasound gain +27 dB, PA gain 25 dB, priority 95%, distance 1.2–1.5 cm from the transducer. PA average (Average PA intensity (arbitrary units, AU) were computed by the built-in imaging software using photoacoustic intensity per unit two-dimensional area. 3D-mode testing of ISCs (with different concentrations of ICG) was performed on the phantom demonstrating increased PA intensity with concentration. The LZ550 transducer was utilized (Axial resolution 44 um, broadband frequency 32–55 MHz).

ISCs were intravenously (orbital) injected into mice bearing U251 (+Luc) flank xenografts. Twenty-four hours following injection (1 mg/kg based on ICG weight), the animals were imaged with excitation at 850 nm with the following parameters: ultrasound gain +27 dB, PA gain 25 dB, priority 95%. 1 mg/kg was chosen as a candidate dose based on human

dosing for solid tumor imaging and previously published data on ICG and iron oxide dosing required for MR imaging[14–16].

Surgical Resection Trial

Twenty-four mice (N=24) were implanted with U251 (+Luc) cells expressing as above and randomized to either a photoacoustic (PA)-guided surgery arm (N=12) or microscopic resection arm (N=12). The animals in both groups undergoing surgery had operations performed using 3.5X loupe magnification and white light, once the tumors reached >7mm in their largest dimension. The PA-guided surgery arm underwent Photoacoustic imaging studies done as part of surgery to identify areas of residual tumor following initial resection. Following surgery, all animals were identified/tagged and monitored for recurrence by a different individual than the operating surgeon at varying timepoints to assess for survival and progression of disease. Animals were injected with 1 mg/kg ISCs based on ICG weight (intraorbital) and imaged 24 hours following injection as above. For all animals, PA imaging parameters were kept constant (ultrasound gain +27 dB, PA gain 25 dB, priority 95%) including time-gain constant.

Progression-free survival data in both groups was calculated based on periodic assessments with bioluminescence imaging as previously described. Timepoints for intraperitoneal injection of D-Luciferin (to assess recurrence) were at 0, 10, 25, and 42 days for the microscopic surgery cohort and at 0, 12, 25, and 42 days for the PA-guided surgery cohort. Bioluminescence studies were performed 12 minutes following IP injection of D-luciferin sodium salt based on peak signal time (200 uL, 15 mg/ml intraperitoneal injection)[47]. Animals were monitored for pain (as above) and treated appropriately as per the IRB/IACUC protocol. Kaplan-Meier and log-rank statistical analyses were performed in Stata v. 12.

Supplementary Material

Refer to Web version on PubMed Central for supplementary material.

Acknowledgments

This work was supported by NIH/NIBIB (U01-EB016027) and NIH/NCI (R01-CA181429 and R01-CA175480)

References

1. Brem S, Abdullah KG. Glioblastoma. n.d
2. Lacroix M, Abi-Said D, Fourney DR, Gokaslan ZL, Shi W, DeMonte F, Lang FF, McCutcheon IE, Hassenbusch SJ, Holland E, Hess K, Michael C, Miller D, Sawaya R. J Neurosurg. 2001; 95:190.
3. Stummer W, Pichlmeier U, Meinel T, Wiestler OD, Zanella F, Reulen H-J. Lancet Oncol. 2006; 7:392. [PubMed: 16648043]
4. Sanai N, Berger MS. Neurosurgery. 2008; 62:753. [PubMed: 18496181]
5. Bloch O, Han SJ, Cha S, Sun MZ, Aghi MK, McDermott MW, Berger MS, Parsa AT. J Neurosurg. 2012; 117:1032. [PubMed: 23039151]
6. Chaichana KL, Jusue-Torres I, Navarro-Ramirez R, Raza SM, Pascual-Gallego M, Ibrahim A, Hernandez-Hermann M, Gomez L, Ye X, Weingart JD, Olivi A, Blakeley J, Gallia GL, Lim M, Brem H, Quinones-Hinojosa A. Neuro Oncol. 2014; 16:113. [PubMed: 24285550]

7. Almenawer SA, Badhiwala JH, Alhazzani W, Greenspoon J, Farrokhyar F, Yarascavitch B, Algird A, Kachur E, Cenic A, Sharieff W, Klurfan P, Gunnarsson T, Ajani O, Reddy K, Singh SK, Murty NK. Neuro Oncol. 2015; 17:868. [PubMed: 25556920]
8. Nguyen QT, Tsien RY. Nat Rev Cancer. 2013; 13:653. [PubMed: 23924645]
9. Azzopardi E, Owens S, Murison M, Rees D, Anne Sawhney M, Francis L, Sofia Rodrigues Texeira R, Clement M, Steven Conlan R, Whitaker I. J Control Release. 2017; doi: 10.1016/j.jconrel.2016.12.044
10. Levesque E, Martin E, Dudau D, Lim C, Dhonneur G, Azoulay D. Anaesth Crit Care Pain Med. 2016; 35:49. [PubMed: 26477363]
11. Ebert B, Riefke B, Sukowski U, Licha K. J Biomed Opt. 2011; 16:66003.
12. Marshall MV, Rasmussen JC, Tan I-C, Aldrich MB, Adams KE, Wang X, Fife CE, Maus EA, Smith LA, Sevick-Muraca EM. Open Surg Oncol J. 2010; 2:12. [PubMed: 22924087]
13. Predina JD, Judy B, Fridlender ZG, Aliperti LA, Madajewski B, Kapoor V, Cheng G, Quatromoni J, Okusanya O, Singhal S. Cancer Biol Ther. 2012; 13:745. [PubMed: 22617772]
14. Madajewski B, Judy BF, Mouchli A, Kapoor V, Holt D, Wang MD, Nie S, Singhal S. Clin Cancer Res. 2012; 18:5741. [PubMed: 22932668]
15. Holt D, Okusanya O, Judy R, Venegas O, Jiang J, DeJesus E, Eruslanov E, Quatromoni J, Bhojnagarwala P, Deshpande C, Albelda S, Nie S, Singhal S. PLoS One. 2014; 9:e103342. [PubMed: 25072388]
16. Lee JYK, Thawani JP, Pierce J, Zeh R, Martinez-Lage M, Chanin M, Venegas O, Nims S, Learned K, Keating J, Singhal S. Neurosurgery. 2016; 79:856. [PubMed: 27741220]
17. Wang LV, Hu S. Science (80-). 2012; 335:1458.
18. Kircher MF, de la Zerda A, Jokerst JV, Zavaleta CL, Kempen PJ, Mittra E, Pitter K, Huang R, Campos C, Habte F, Sinclair R, Brennan CW, Mellinghoff IK, Holland EC, Gambhir SS. Nat Med. 2012; 18:829. [PubMed: 22504484]
19. Zhang Y, Hong H, Cai W. Cold Spring Harb Protoc. 2011; 2011doi: 10.1101/pdb.top065508
20. Gao C, Deng Z-J, Peng D, Jin Y-S, Ma Y, Li Y-Y, Zhu Y-K, Xi J-Z, Tian J, Dai Z-F, Li C-H, Liang X-L, Gao C, Deng Z-J, Peng D, Jin Y-S, Ma Y, Li Y-Y, Zhu Y-K, Xi J-Z, Tian J, Dai Z-F, Li C-H, Liang X-L. Cancer Biol Med. 2016; 13:349. [PubMed: 27807502]
21. Cheng Z, Al Zaki A, Hui JZ, Tsourkas A. Anal Chem. 2012; 84:7578. [PubMed: 22882145]
22. Joh DY, Sun L, Stangl M, Al Zaki A, Murty S, Santoiemma PP, Davis JJ, Baumann BC, Alonso-Basanta M, Bhang D, Kao GD, Tsourkas A, Dorsey JF. PLoS One. 2013; 8:e62425. [PubMed: 23638079]
23. Singhal S, Holt D, Nie S, Wang MD, Madajewski B, Judy BF, Mouchli A, Kapoor V. Clin Cancer Res. 2012; 18:5741. [PubMed: 22932668]
24. Ma Y, Tong S, Bao G, Gao C, Dai Z. Biomaterials. 2013; 34:7706. [PubMed: 23871538]
25. Zheng X, Xing D, Zhou F, Wu B, Chen WR. Mol Pharm. 2011; 8:447. [PubMed: 21197955]
26. Zheng X, Zhou F, Wu B, Chen WR, Xing D. Mol Pharm. 2012; 9:514. [PubMed: 22332810]
27. Orringer DA, Golby A, Jolesz F. Expert Rev Med Devices. 2012; 9:491. [PubMed: 23116076]
28. Nabavi A, Black PM, Gering DT, Westin CF, Mehta V, Pergolizzi RS, Ferrant M, Warfield SK, Hata N, Schwartz RB, Wells WM, Kikinis R, Jolesz FA. Neurosurgery. 2001; 48:787. [PubMed: 11322439]
29. Hirschberg H, Samset E, Hol PK, Tillung T, Lote K. min - Minim Invasive Neurosurg. 2005; 48:77. [PubMed: 15906201]
30. Schatlo B, Fandino J, Smoll NR, Wetzel O, Remonda L, Marbacher S, Perrig W, Landolt H, Fathi A-R. Neuro Oncol. 2015; 17:1560. [PubMed: 25858636]
31. Stummer W, Tonn J-C, Goetz C, Ullrich W, Stepp H, Bink A, Pietsch T, Pichlmeier U. Neurosurgery. 2014; 74:310. [PubMed: 24335821]
32. Zhao S, Wu J, Wang C, Liu H, Dong X, Shi C, Shi C, Liu Y, Teng L, Han D, Chen X, Yang G, Wang L, Shen C, Li H. PLoS One. 2013; 8doi: 10.1371/journal.pone.0063682
33. Gordon DL, Airan MC, Thomas W, Seidman LH. Br J Surg. 1975; 62:747. [PubMed: 51661]
34. Bajwa A, Aman R, Reddy AK. Int Ophthalmol. 2015; 35:733. [PubMed: 26043677]

35. Gao H, Cao S, Chen C, Cao S, Yang Z, Pang Z, Xi Z, Pan S, Zhang Q, Jiang X. Nanomedicine (Lond). 2013; 8:1429. [PubMed: 23451915]
36. Wei F, Wang Q, Su Q, Huang H, Luan J, Xu X, Wang J. Cell Mol Neurobiol. 2016; 36:1389. [PubMed: 26858153]
37. Deng Y, Li W, Li Y, Yang H, Xu H, Liang S, Zhang L, Li Y. Oncol Rep. 2010; 23:69. [PubMed: 19956866]
38. Zhang H, Nie W, Zhang X, Zhang G, Li Z, Wu H, Shi Q, Chen Y, Ding Z, Zhou X, Yu R. PLoS One. 2013; 8:e82789. [PubMed: 24340059]
39. McQuade C, Al Zaki A, Desai Y, Vido M, Sakhuja T, Cheng Z, Tsourkas A, Hickey RJ, Joh D, Kao G, Dorsey JF, Park SJ. Small. 2015; 11:834. [PubMed: 25264301]
40. Xie J, Peng S, Brower N, Pourmand N, Wang SX, Sun S. Pure Appl Chem. 2006; 78:1003.
41. Sun S, Zeng H, Robinson DB, Raoux S, Rice PM, Wang SX, Li G. J Am Chem Soc. 2004; 126:273. [PubMed: 14709092]
42. Ciapetti G, Cenni E, Pratelli L, Pizzoferrato A. Biomaterials. 1993; 14:359. [PubMed: 8507779]
43. Gao L-B, Tian S, Gao H-H, Xu Y-Y. Neuroreport. 2013; 24:504. [PubMed: 23660683]
44. Baumann BC, Dorsey JF, Benci JL, Joh DY, Kao GD. J Vis Exp. 2012; doi: 10.3791/4089
45. Jacobs VL, Valdes PA, Hickey WF, De Leo JA. ASN Neuro. 2011; 3:e00063. [PubMed: 21740400]
46. Husain SR, Behari N, Kreitman RJ, Pastan I, Puri RK. Cancer Res. 1998; 58:3649. [PubMed: 9721874]
47. Baumann BC, Dorsey JF, Benci JL, Joh DY, Kao GD. J Vis Exp. 2012; doi: 10.3791/4089

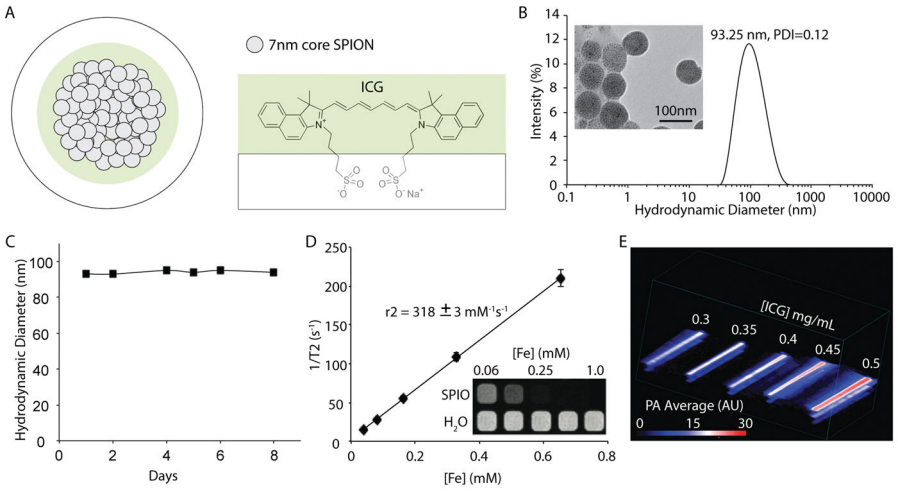

Figure 1.

(A) Schematic representation of ICG SPIO clusters (ISCs). Iron oxide nanoparticles are self-assembled using a microemulsion technique and stabilized using indocyanine green, an amphiphilic, cyanine dye. (B) Dynamic light scattering (DLS) profile of ISCs. Size distribution by intensity percentage, in water. Transmission electron microscopy (TEM; inset) performed demonstrating spherical, tightly packed clusters with SPIO-NP cores (scale bar: 100 nm). (C) Particle size based on mean intensity (%) measurements (DLS) taken over a total of 8 days, in water at 25°C. (D) Magnetic resonance (MR) relaxometry measurements of ISCs. MR phantom image (inset) of ISCs at various concentrations in a microplate. (E) Photoacoustic phantom of ISCs, demonstrating increased PA intensity with concentration. Testing performed in 0.5 mm diameter polyethylene tubing submerged in milk, depth between 1–2 cm. PA averages (Average PA intensity (arbitrary units, AU) are computed using photoacoustic intensity per unit volume at 850 nm excitation.

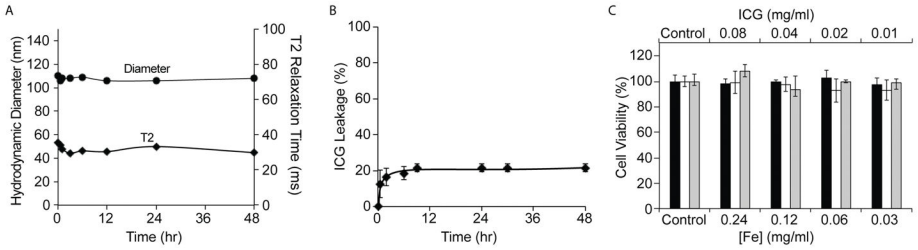

Figure 2.

(A) ISCs were incubated in serum, at 37°C, and dynamic light scattering (DLS) and relaxometry measurements were recorded as a function of time. (B) Release of ICG from ISCs was monitored as a function of time following addition to serum, at 37°C (C) Proliferation of human embryonic kidney (HEK) 293T cells (black bar), human umbilical vein endothelial cells (HUVEC) (white bar), and U251 glioblastoma cells (gray bar) was assessed via an MTT assay, after incubation with increasing concentrations of ISCs for 24 hrs.

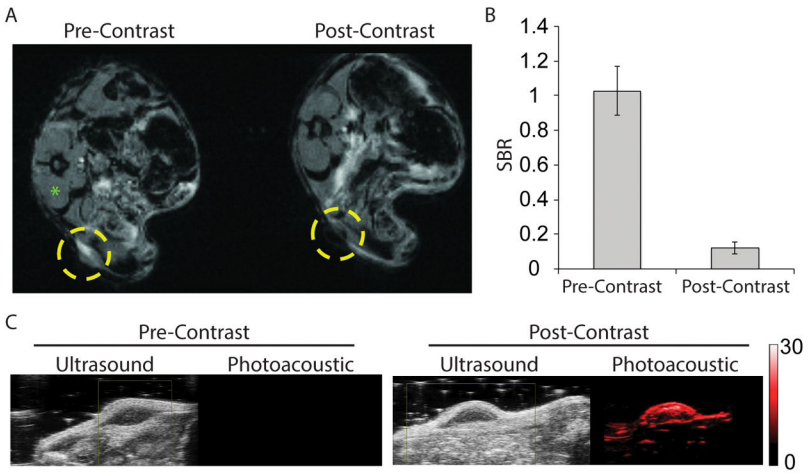

Figure 3.

(A) T2-weighted magnetic resonance (MR) imaging before (left) and 24 hours after (right) intravenous (intraorbital) injection of 1mg/kg ISCs by ICG weight into mice bearing U251 flank xenografts. Yellow circles denote the location of the flank tumor. (B) Signal-to-background ratio (SBR) measurements were made using the candidate tumor and the paraspinous musculature (green asterisk) as background. Pre-injection versus post-injection SBR measurements are shown. (C) Ultrasound and Photoacoustic imaging before (left) and 24 hours after (right) intravenous (intraorbital) injection of 1 mg/kg ISCs by ICG weight into a mouse bearing U251 flank xenograft tumor. ISCs were noted at a red-shifted wavelength (850 nm) relative to the fluorescence spectra of ICG.

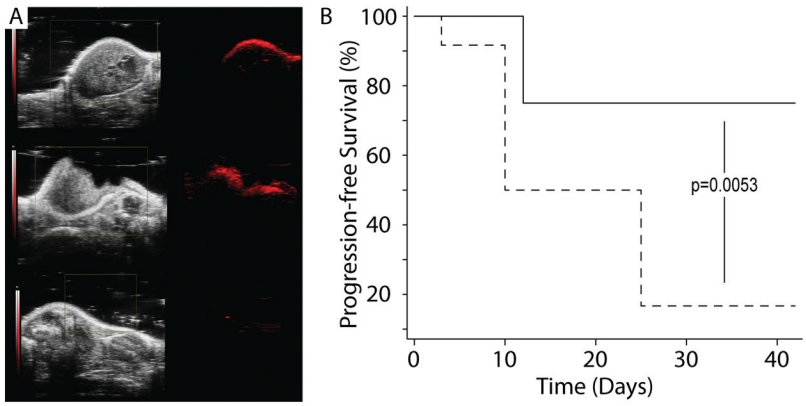

Figure 4.

(A) Animals were injected with 1 mg/kg ISCs and imaged 24 hours following injection. Left panels show ultrasound imaging as seen using the Photoacoustic imaging platform. Right panels show photoacoustic imaging (PA) data obtained following injection. Pre-operative PA imaging with excitation at 850 nm demonstrates signal within the tumor (top). Following surgical debulking, persistent PA signal is notable at the resection cavity (middle). Following complete excision, saline irrigation, and skin closure, low residual PA signal is noted (bottom). (B) Surgical resection trial. Twenty-four mice (N=24) were implanted with U251 cells expressing luciferase (U251 +Luc) and randomized to either a PA-guided surgery arm (N=12, solid line) or microscopic surgical resection arm (N=12, dashed line). Following surgery, all animals were identified/tagged and monitored for recurrence at varying time points to assess for survival and progression of disease.